Experimental Investigation of Wire Mesh Sensors (WMS) for Void Measurement and Visualization

Roshini Robin[1,*], Rajalakshmi.R[1,*]
[1]Reactor Engineering Division, Bhabha Atomic Research Centre, Mumbai 400 085
[*]Email: rajlaxmi@barc.gov.in, Ph: 022-25595154
roshini@barc.gov.in, Ph: 022-25591620

ABSTRACT

The study of two phase flow behavior has gained importance in BWR type nuclear power plants to enhance fuel performance and safety. In the analysis of the two phase flow system, an accurate prediction of void distribution through measurements and visualization is very important to enhance critical heat flux and to improve nuclear safety and fuel economy. Thus the sensor development for the measurement and visualization of void profile is of greater concern. In the view of the above, in this paper, electrical sensors such as Wire Mesh Sensors (WMS) is designed for measurement of void distribution and its visualization. WMS works on the conductivity principle and the flow distributions are identified by measuring the variations in conductivity values of the two phases. As WMS measures the void distribution along the cross-section of the pipe, they can be considered as flow imaging devices. An 8X8 WMS along with its electronics unit has been designed and fabricated in-house for experiments in the Air-Water two phase test facility loop in BARC. The WMS experimental data for different flow regimes such as bubbly, slug and churn flows were compared with the co-relation models for investigating the performance of the sensor. The CFD simulations of the two phase flow were coupled with the sensor AC/DC module in the COMSOL FEM software for validating the experimental data with the simulation results. Different image reconstruction and visualization methods are discussed for two phase flow visualization and void distribution studies. Suitable algorithm and programming were developed and discussed for the visualization from WMS experimental data.

KEYWORDS

Void fraction, bubbly flow, slug flow, churn flow, two phase visualization, superficial velocity.

INTRODUCTION

WMS are based on the measurement of the local instantaneous conductivity of the two-phase mixture. It comprises of two set of wires stretched over the cross-section of a vessel or pipe. The planes of wires are perpendicular to each other and forming a grid of electrodes. The associated electronics measures an electrical property of the flowing media at each crossing point in a very fast and multiplexed manner.

The wire mesh subdivides the flow channel cross section into a number of independent sub-regions, whereas each crossing point represents one sub-region. Each of the measured signals reflects the constitution of the flow within its associated sub-region, i.e. each crossing point acts as local phase indicator. Hence, the set of data obtained from the sensor directly represents the phase distribution over the cross-section.

SENSOR WORKING PRINCIPLE

The simplified diagram of the WMS is shown in Fig. 1. During the measuring cycle, the transmitter electrodes are activated by a multiplex circuit in a successive order, as illustrated in **Fig.1**.

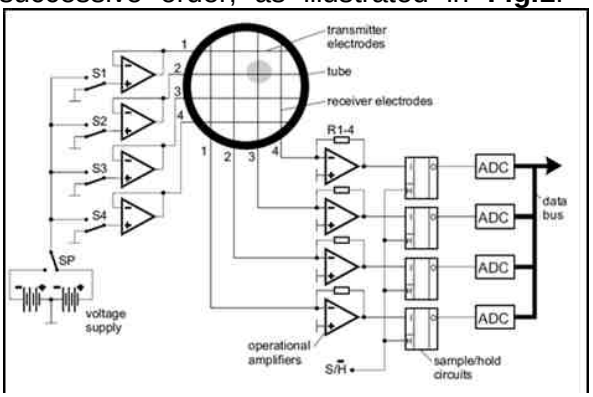

Figure 1- Simplified scheme of a two 4X4 WMS with signal acquisition system

The excitation is done by DC-free symmetrical rectangular pulses. The currents arriving at the receiver wires are transformed into voltages by operational amplifiers and sampled by individual sample/hold circuits and stored by ADC. After an analogue/digital conversion the signals are recorded by a data acquisition computer and stored for each receiver electrode separately.

The activation procedure is repeated for all transmitter electrodes. After activating the last transmitter wire, a complete matrix of measured values is stored in the computer, which represents the complete two dimensional conductivity distributions in the sensor cross section at the time of measurement. During the activation of a single transmitter electrode and all the other electrodes are kept on zero potential. This prevents a deterioration of the resolution by cross talk between parallel wires.

EXPERIMENTAL SETUP

The experiments were done at the Air Water two phase test facility. The schematic drawing of the experimental test facility is shown in **Fig. 2**.

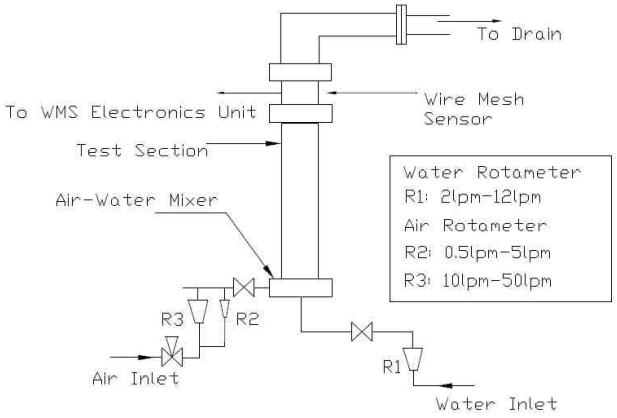

Figure 2- Schematic drawing of WMS Experimental Test Facility

The facility consists of a vertical test section of an acrylic circular pipe of 2 meter height and 50 mm ID. Air and water are separately injected through the bottom of the test section. Water is pumped from the bottom of the test facility and mixes with the air bubbles in the air-water mixer before entering the test section. The two phase mixture is then left to drain from the top at the exit of the test section. The process water used in the test facility for the experiments was tap water. Separate flow meters are installed in the air and water inlet lines to measure air and water flow rate respectively. Flow meter of 2 lpm to 12 lpm range is installed for the water flow rate measurements. Two flow meters for coarse flow rate (10 lpm to 50 lpm range) and fine flow rate (0.5 lpm to 5 lpm) is installed for air flow rate measurements. WMS is installed at the exit of the test section between two flanges as shown in the Figure 2. The transmitter and the receiver sensor leads of the WMS are connected to the WMS electronics unit through an 8 core shielded copper wire. The pressure during the experiment is

maintained at 10 psi. The different flow regimes of bubbly, slug and churn flow were created by varying the air flow rates and maintaining the water flow rate at a constant value.

The complete WMS experimental set-up including the Air-Water two phase test facility with the WMS installed, the WMS electronics unit and the data acquisition are shown in **Fig. 3**.

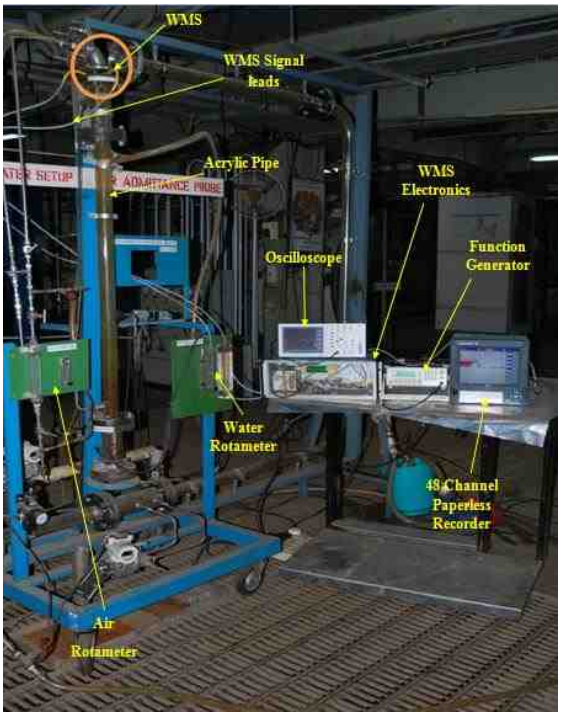

Figure 3- WMS experimental setup with sensor electronics

The sensor mounted in the test facility between two flanges is shown separately in **Fig. 4**. An 8 by 8 wire mesh sensor was fabricated in an acrylic rectangular frame block of 80mm X 80mm X 23mm dimensions. Stainless steel was considered as the WMS material owing to its high conductivity and high tensile strength. The fabricated sensor is shown in **Fig. 4**. There are 8 transmitter- receiver electrode pairs which are connected to 8 channel WMS electronics unit.

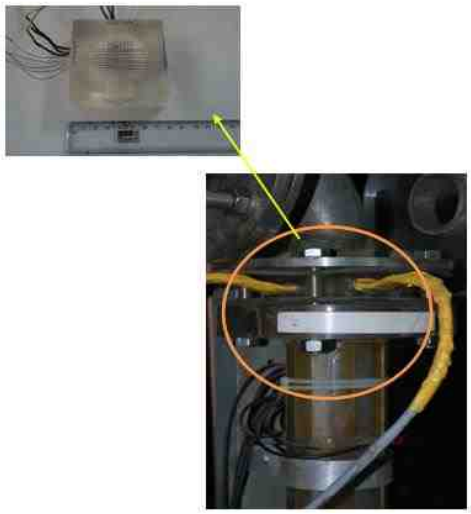

Figure 4- WMS mounted in the air-water two phase test facility

The bipolar square wave voltage excitation for the sensor is given from function generator. The WMS electronics unit has a WMS excitation circuit and a signal conditioning circuit. The block diagram of the WMS electronics is shown in **Fig. 5**. The excitation signal is multiplexed to the WMS transmitter leads using WMS switching circuit one at a time while the others are being grounded. The control signals for switching are provided by programming microcontroller IC. The current output signals from the WMS receiver leads are converted to voltage signals, rectified and filtered using the signal conditioning circuit. The output data from the sensor electronics unit are recorded for WMS data analysis.

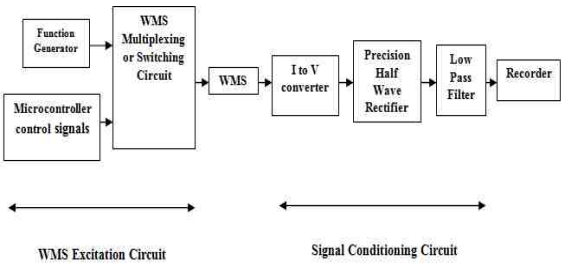

Figure 5- Block diagram of WMS electronics

The 3D view of the PCB designed and fabricated for the WMS electronics unit is shown in **Fig. 6**. The PCB of WMS excitation and signal conditioning unit, power supply and display are mounted in a 19" bin.

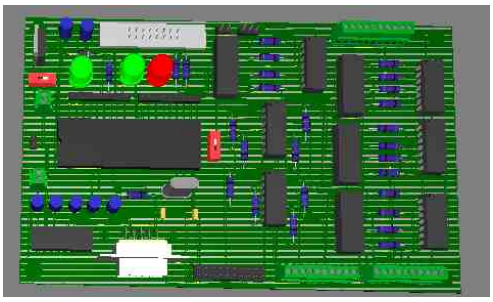

Figure 6- 3D view of the PCB designed in the simulation software

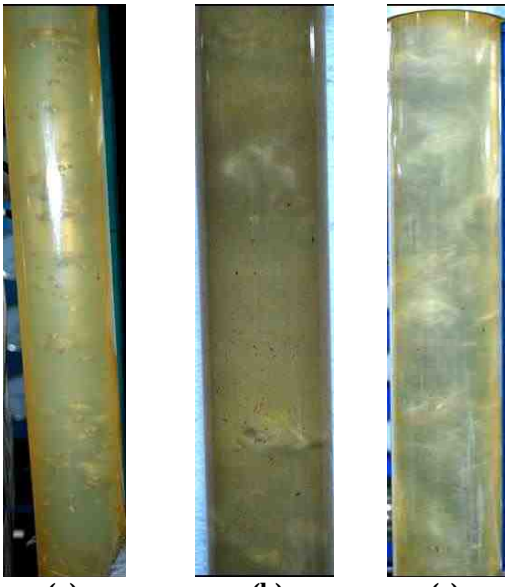

(a) **(b)** **(c)**

Figure 7- (a) Bubbly flow regime (α=10.543%) (b) Slug flow regime (α=36.189%) (c) churn flow regime (α=45.467%)

Experiments were conducted for 10% to 60% void fractions covering the bubbly, slug and churn flow regimes. The different flow regimes were created by varying the flow rate of air and maintaining a constant water flow rate. The different flow regimes created were captured using a high resolution camera. The images captured are shown in **Fig. 7**.

EXPERIMENT RESULTS

- **Comparison of the WMS Experimental data with the Co-relation model**

The total time averaged void fractions were calculated from the experimental data for bubbly, slug and churn flow regimes by varying gas phase superficial velocities. The WMS output voltages at each local sensor cross over points for all the 2D time frames $V_k\ (i\ ,\ j)$ were converted to their equivalent local void fractions $\alpha_x\ (i\ ,\ j)$ using linear calibration model. For this linear calibration model, the voltages for 0% void fraction was taken for the sensor fully filled with water and the voltages for 100% void fraction was taken with experimental case of water flow rate of 4lpm and air flow rate of 10 lpm.

The calculations for total time averaged void fractions were done in accordance with the formula as given below:

$$\bar{\alpha} = \frac{1}{k_{max}} \sum_{i=1}^{i_{max}} \sum_{j=1}^{j_{max}} \sum_{k=1}^{k_{max}} a_{i,j} . \alpha_{i,j} = \sum_{i=1}^{i_{max}} \sum_{j=1}^{j_{max}} a_{i,j} . \overline{\alpha_{i,j}}$$

Where, the weight coefficients $a_{i,j} = \Delta x . \Delta y / A_{sensor}$. Δx and Δy are the spatial resolution of the designed WMS and A_{sensor} is the WMS area.

The void fractions for different flow regimes were calculated by maintaining a constant water superficial velocity and by varying the gas superficial velocities from 8.5E-3 m/s to 4.2E-2 m/s. The void fractions obtained from the WMS experimental data was compared with the Chisholm's correlation model as in **Fig. 8**. The profile of the experimental data matches with the correlation data. The experimental data exceeds the correlation values with an error of 10% for the gas superficial velocities upto 3.4E-2 m/s. For higher gas

superficial velocities, the deviation increases due to the regime dependency of the correlation model.

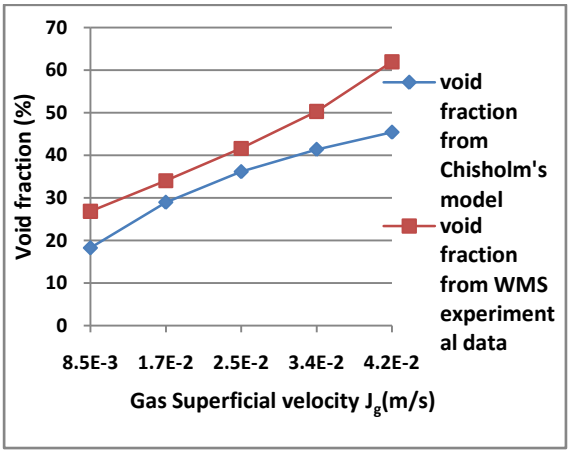

Figure 8- Void fraction from the Chisholm's model and WMS experimental data for different gas superficial velocities

Fig. 9 gives the comparison plot between the experimental void fractions calculated from the WMS output and the expected values from the Chisholm's correlation model. The experimental data matches linearly with the expected correlation data.

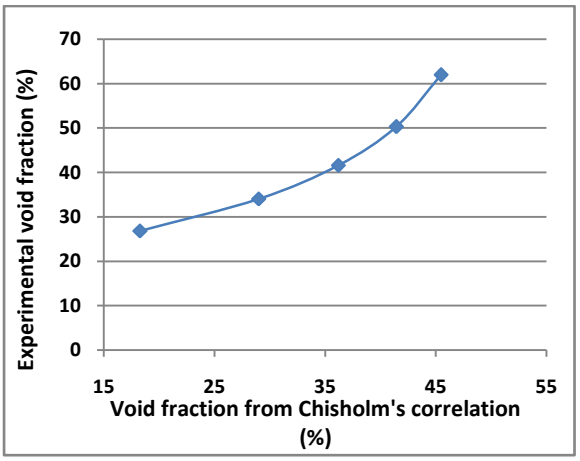

Figure 9- WMS experimental Vs Chisholm's correlation void fraction data

- **Comparison of WMS Experimental data with Simulation results**

Local voltage calculations were done at each sensor cross-over points for the full water and bubbly flow case both from experimental data and simulation data from the FEM software by coupling the COMSOL-CFD module with the COMSOL-AC/DC module. Local time averaged voltage calculations were done for the 2D time frames. The relation for the 2D time averaged voltage distribution is given below:

$$\overline{V_{i,j}} = \frac{1}{k_{max}} \sum_{k=1}^{k_{max}} V_{i,j,k}$$

k_{max} is the total number of time frames up to which measurement is taken. *i* and *j* are the x and y sensor cross-over point locations. The plots for the 2D time averaged voltage distribution at each sensor cross-over points of the third transmitter wire for 0% and 10.54% void fraction are given in **Fig. 10**.

From the comparison plots in Figure 10 between the experimental and the simulation data's, the voltage trends obtained from the experimental data, matches well with the simulation results for the sensor cross-over grid locations.

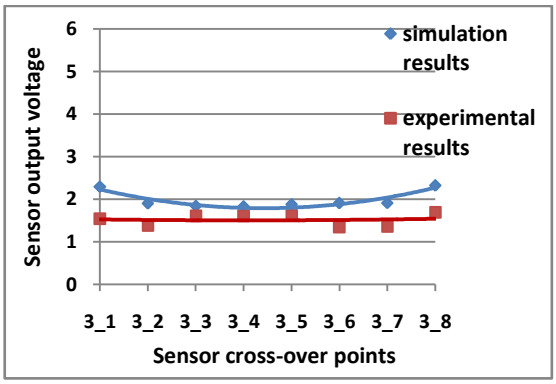

(a)

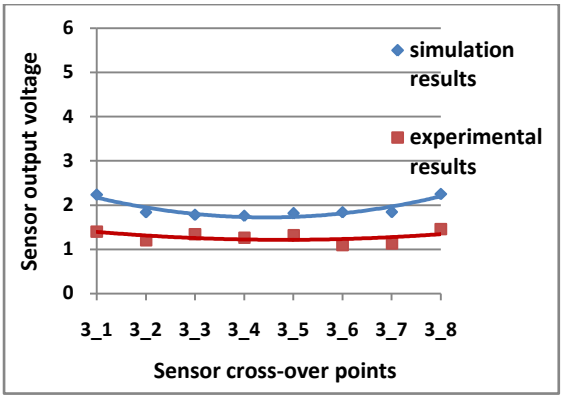

(b)

Figure 10- Comparison between the FEM simulation and WMS experimental results of local time averaged voltage values at each sensor cross-over point of the 3rd transmitter wire for (a) 0% void fraction (b) 10.54% (bubbly flow) void fraction

However, the value of the measured experimental voltage data is lower than the FEM simulation data with an error of 25% for the 0% void fraction case and 33% for the 10.53% void fraction case respectively. Thus based on these comparison results, WMS are feasible for two phase flow measurements.

IMAGE RECONSTRUCTION AND VISUALIZATION

The data evaluation starts from the transformation of the instantaneously measured electrical signals into local instantaneous gas fractions**.** The result is a matrix of local instantaneous volumetric gas fractions α(*i*, *j*,*k*) where, *k* is the number of the current measurement and *i* and *j* are the indexes of the location in the sensor plane. These data can be used to calculate cross-section averaged gas fractions and for the visualization of instantaneous local voids.

Three different image visualization methods [4], [5], [6], [7] that can be applied to visualize the resulting gas fraction matrix α(*i*, *j*, *k*) are discussed below.

a) Instantaneous gas fraction distributions in the measuring plane:

These distributions are obtained by plotting 2-D distributions in the directions of *i* and *j* for a fixed value of index *k*. Sequences of these distributions obtained by stepwise incrementing index *k* can be viewed as animated images.

b) Virtual sectional side views:

In the case of the virtual sectional side views, a distribution either in the plane *i*, *k* or *j*, *k* is plotted on the screen in such a way that the time axis is oriented downward. The third index is kept constant, usually at a value representing an electrode wire in the centre of the cross section. Such an image obtains the character of a side view to the flow on a vertical plane cut through the pipe along the diameter. The vertical axis can be transformed into a virtual *z* axis when it is scaled according to the velocity of the gaseous phase. Since individual bubble velocities are not available, the average phase velocity calculated from the known superficial gas velocity divided by the measured average gas fraction can be used as an approximation so as to obtain an approximate visualization of the real shape of the bubbles. This method has the biggest advantage that sectional plots obtained at different airflow rates can be directly compared.

c) Virtual side projections:

This method is applied using a simplified ray-tracing algorithm. For this a virtual light propagation through the three dimensional (3D) column of elements filled either with gas or with liquid according to the gas fraction matrix α (*i*, *j*, *k*) is simulated numerically. The procedure starts with the assumption of parallel white light arriving in the direction of the *x* axis. The light flux is treated like a vector consisting of three components for red, green, and blue. The

white value is 255(i.e., red=blue=green=255) in true-colour bitmap images. It is used as the initial value. When the light penetrates through the column, its red, green, and blue components are partially absorbed by gas and liquid in a selective way. This can be numerically simulated by defining virtual absorption coefficients for each RGB component both for gas and liquid phases individually. In the result of illumination and absorption, there is light of a certain intensity and colour present in each location.

$$\overrightarrow{\phi_{x,i,j}} = \overrightarrow{\phi_{x,i-1,j}} * [1 - \overrightarrow{\Lambda_{gas}} * \varepsilon_{i,j} - \overrightarrow{\Lambda_{liquid}} * (1 - \varepsilon_{i,j})] \quad (9.1)$$

Where, $\phi_{x,i,j}$ is the light flux along the x-axis direction for deferent i , j values along the sensor, $\overrightarrow{\Lambda_{gas}}$ and $\overrightarrow{\Lambda_{liquid}}$ are the absorption coefficients for the gas and liquid phase respectively.
In the next step it is assumed that the gas and the liquid scatter a portion of this intensity towards the observer. This is reflected by a source term as given below:

$$\overrightarrow{Q_{i,j}} = \overrightarrow{\phi_{x,i,j}} * [\overrightarrow{\Omega_{gas}} * \varepsilon_{i,j} - \overrightarrow{\Omega_{liquid}}(1 - \varepsilon_{i,j})] \quad (9.2)$$

Where, $\overrightarrow{Q_{i,j}}$ is the source term, $\overrightarrow{\Omega_{gas}}$ and $\overrightarrow{\Omega_{liquid}}$ are the virtual scattering coefficients of gas and liquid respectively. The virtual absorption coefficients and the virtual scattering coefficients are to be chosen empirically so as to optimize the visual impression of the achieved imaging so that gas and liquid phases can be visualised separately with appropriate colours. From this visualisation method, we can obtain an image of the flow pattern, which is close to a visual observation through a transparent pipe wall.

VISUALIZATION FROM WMS EXPERIMENTAL DATA

The image processing for the image reconstruction and visualization from the experimental data were done for different gas-phase superficial velocities corresponding to the various two phase flow regimes. Image processing was done on each 2D WMS output electrical data frames so as to obtain the visualization of void fraction distributions. The programming for image processing was done using the image processing toolbox from the available simulation software. Each of these image processed 2D data frames were converted to its equivalent 3D void distribution in a vertical pipe using Virtual Side Sectional Projections methods. The programming for the 3D mapping and visualization were done using the same Simulation software.

The void fraction data frames were recorded with 4s during the field experiments for different gas phase superficial velocities. The virtual side section projection output for a constant water phase superficial velocity of 0.0339m/s and different gas phase velocities from 0.0042 m/s to 0.0424 m/s with corresponding void fractions of 11%, 20%, 33%, 42.85%, 50% and 55% are shown in **Fig.11**. From these image processed data outputs, the small bubbles and the larger slugs for increasing gas phase superficial velocities could be successfully recreated for void distribution visualization.

Figure 11- Image processed output data for different void fractions (a) α=11% (b) α=20% (c) α=33% (d) α=42.85% (e) α=50% (f) α=55.5%.

RESULTS AND CONCLUSIONS

WMS has been designed, tested and experimented for void fraction measurements and visualization for two phase flow in a 50NB vertical pipe in air-water two phase test facility loop in BARC. A prototype WMS along with its electronics unit was designed and fabricated in-house for experimentation. The WMS experimental data were compared with correlation models and COMSOL simulation results for validation of sensor. Image processing algorithm and programming for the visualization of void distribution from the experimental data for different air and water superficial velocities has been developed and discussed. Thus from the simulation studies and the experimental results discussed in this paper, WMS are suitable for two phase void fraction measurements and visualization.

NOMENCLATURE

1. Y_x – Admittance of the two phase mixture
2. G_x - Conductance of the two phase mixture
3. C_x - Capacitance of the two phase mixture
4. ε_r - Relative dielectric constant
5. ε_0 - Vacuum permittivity
6. k_g - Geometry factor of the sensor cross-over point
7. Y_f – Feedback admittance
8. V_i – Sensor excitation signal
9. G_f – Feedback conductance
10. V_0 – Sensor output voltage
11. i ,j – Indices of the WMS cross-over points
12. $V_k(i,j)$- 2D sensor output voltage at each sensor cross-over point
13. $\overline{V_{i,j}}$ – local time averaged voltage
14. k – Time index
15. $\alpha_x\ (i,j,k)$ – 2D local void fraction distribution for the k^{th} time frame
16. Δx, Δy – Electrode pitches
17. f_m – Measuring frequency
18. Δt – time step
19. $\overline{\alpha_{i,j}}$ – Time average 2D void fraction distribution
20. A_{sensor} – Total sensor cross-sectional area
21. $a_{i,j}$ - Sensor weight coefficients
22. μ – magnetic permeability
23. σ – Electrical conductivity
24. V – Electrical potential
25. E – Electrical field
26. u_l – Liquid phase velocity vector
27. ϕ_l - Liquid phase void fraction
28. ρ_l - Density of the liquid phase
29. μ_l – Dynamic viscosity of the liquid phase
30. ϕ_g – Gas phase void fraction
31. ρ_g – Density of the gas phase
32. u_g – Gas phase velocity vector
33. μ_g – Dynamic viscosity of the gas phase
34. S – Spatial sensitivity of the sensor
35. ΔZ - Change in sensor impedance due to the presence of perturbation
36. J_g – Gas superficial velocity
37. J_l – Liquid superficial velocity

REFERENCES

[1] Lucas G.P., Cory J., Waterfall R.C., Loh W.W., and Dickin F.J. (1999), Measurement of

the solids volume fraction and velocity distributions in solids–liquid flows using dual-plane electrical resistance tomography. *Flow Measurement and Instrumentation* **10** 249–258.

[2] H.-M. Prasser, A. Böttger, J. Zschau (1998), A new electrode-mesh tomograph for gas-liquid flows. *Flow Measurement and Instrumentation* **9** 111-119.

[3] H.F. Velasco Pena, O.M.H. Rodriguez. (2015), Applications of Wire Mesh Sensors in Multiphase Flows. *Flow Measurement and Instrumentation* **45** 255-273.

[4] H.M. Prasser, M. Beyer, A. Bottger, H. Carl, D. Lucas, A. Schaffrath, P. Schutz, F.P. Weiss, and J. Zschau (2004), Influence of the pipe diameter on the structure of the gas-liquid interface in a vertical two phase pipe flow, *FZR, Institute of Safety Research.*

[5] A. Manera, H.M. Prasser, D. Lucas, T.H.J.J. van der Hagen (2006), Three Dimensional Flow Pattern Visualization and Bubble Size Distributions in Stationary and Transient Upward Flashing Flow, *International Journal of Multiphase Flow* **32** 996-1016

[6] H.M. Prasser, D. Scholz, C. Zippe (2001), Bubble Size Measurement using Wire Mesh Sensors, *Flow Measurement and Instrumentation* **12** 299-312.

[7] H.M. Prasser, Eckhard Krepper, Dirk Lucas (2002), Evolution of the two phase flow in a vertical tube – decomposition of gas fraction profiles according to bubble size classes using wire mesh sensors, *International Journal of Thermal Sciences* **41** 17-28.

[8] INTRODUCTION TO FEM Multiphysics, FEM Software Multiphysics documentation manual.

[9] D. Chisholm, Void fraction during two-phase flow, J. Mech. Eng Sci. 15 (1973) 235-236.